Arabian Journal of Geosciences (2021) 14:734
https://doi.org/10.1007/s12517-021-07014-5

ORIGINAL PAPER

Petrographic, geochemical and structural characteristics of gold-bearing metasedimentary rocks from the Atacora structural unit, Northwestern Bénin Republic

Fatchéssin Bruno Adjo[1,2] · Temidayo Anthony Bolarinwa[1,3] · Luc Adissin Glodji[2] · Prosper M. Nude[4] · Bertrand Anagonou[2] · Jerry Olugbenga Olajide-Kayode[3]

Received: 27 July 2020 / Accepted: 22 March 2021

Abstract

The metasedimentary rocks of the Atacora structural unit around Natitingou in Benin are composed of quartzites, quartz muscovite schist and mica schist. Being auriferous, the petrographic, geochemical and structural features of these rocks were investigated to ascertain the source of gold and its relation to structural deformations. Quartz, muscovite and opaque minerals constitute the dominant minerals in the quartz muscovite schist. The quartzites and mica schists are predominantly composed of quartz, plagioclase, microcline, muscovite and chlorite in varying proportions, with biotite, garnet and epidote in mica schist. The rocks have quartzose sedimentary composition and plot within the passive margin setting on major element discrimination diagrams. The Pan-African ductile and brittle deformation phases produced predominantly folds, strike-slip faults, dextral shear plane and fractures within the area. Gold-bearing veins in the host rocks occur within and near the N-S to NE-SW trending microfolds and the major brittle E-W and NE-SW faults. Gold mineralization is hosted within the NE-trending shear zones and NE-SW trending asymmetric folds which are attributed to transpressional D_2 phase of the Pan-African orogeny. Pathfinder elements for gold mineralization in the Atacora are W–Cu–As–Mo ± Sn. This may suggest interaction between host rocks and mineralizing fluids, probably from deformation and metamorphic processes during the late stages of the Pan-African Orogenic event. However, fluid inclusion and stable isotopic studies are required to constrain the origin of ore fluids.

Keywords Geochemistry · Orogenic gold · Shear zones · Atacora structural unit · Natitingou · Benin · Metasedimentary rocks

Introduction

Metamorphic belts across the world are known to host orogenic gold deposits, accounting for about a quarter of the historic global production of primary gold (Groves et al. 1998; Goldfarb et al. 2005). Although orogenic gold deposits are of great economic importance, a full understanding of the sources of ore fluids and metals continues to be a matter of debate. According to Groves et al. (2003), there are significant parameters concerning orogenic gold deposits, viz. the tectonic setting, mineralogical composition, source of the metals and fluids. These factors are sometimes poorly understood during the exploration phase while they may be compared to those from renowned world-class deposits, thus leading to a better understanding of the gold deposit under investigation.

Assessing the petrochemistry of gold-bearing rocks and structural factors that contribute to gold deposition can be useful for gold exploration, since the chemical composition and structural deformations play relevant roles in mineralization. The understanding of the various structures and their relationships with mineral characteristics is vital to the interpretation of gold mineralization. According to Large et al. (2011), most of orogenic gold deposits across the globe are commonly associated with

Responsible Editor: Domenico M. Doronzo

✉ Fatchéssin Bruno Adjo
afab8213@gmail.com

[1] Department of Geosciences, Pan African University, Life and Earth Sciences Institute (PAULESI), University of Ibadan, Ibadan, Nigeria

[2] Department of Earth Sciences, University of Abomey-Calavi, Abomey-Calavi, Bénin

[3] Department of Geology, University of Ibadan, Ibadan, Nigeria

[4] Department of Earth Science, University of Ghana, Legon, Accra, Ghana

Published online: 16 April 2021

structural deformations and processes of metamorphism, usually with the formation of the ore minerals in terranes of low metamorphic grade. The main orogenic gold deposits are strongly related to deformed metamorphic terranes, with gold commonly related to greenschist facies rocks (Groves et al. 2000; Groves et al. 2003; Goldfarb et al. 2005; Goldfarb and Groves 2015).

Neoproterozoic metasedimentary rocks of greenschist facies, consisting predominantly of quartzites, sandstone and schists are well exposed within the Atacora structural unit (ASU) of the Pan-African Dahomeyides belt in Northwestern Bénin (Affaton et al. 1991), within which the study area is located (Fig. 1b). These rocks were deformed and sheared by many deformational episodes which are evident on the outcrop scale. Gold-bearing quartz veins hosted by these rocks in Northwestern Bénin have been recognized and studied since the colonial era. Previous works on gold mineralization are summarized in Adjo et al. (2019). The genesis and physico-chemical conditions of the palaeo-placer of Perma area (Natitingou) has been examined by Yessoufou et al. (2001), who proposed magmatic origin for the mineralizing fluids. However, disseminated mineralization in the metasedimentary rock units of the area has not yet been documented, with no understanding of their petrogenesis and structural deformations especially their relation to the gold mineralization.

The present study focuses on evaluation of petrographic, geochemical and structural characteristics of gold-bearing quartzites, chlorite–sericite–quartz schists and mica schists within the Natitingou area with the aim of understanding the deformational history and associated gold mineralization. Remobilization of gold from the host rocks during the late stages of the Neoproterozoic Pan-African orogeny is suggested.

Geological setting

The West African Craton is bounded along its margin from north to south and from east to west by five Pan-African mobile belts (Fig. 1a), namely, the Anti-Atlas belt (Hefferan et al. 2000; Ennih and Liégeois 2001), the Rockelides belts (Black et al. 1994), the Pharuside and Dahomeyides belts (Black et al. 1994; Affaton et al. 1991; Abdelsalam et al. 2002) and the Mauritanides belt (Villenenve and Dallmeyer 1987). These belts resulted from an extensive orogenic event during the Neoproterozoic era. During this event, which included ocean opening and closure as well as crustal collision and accretion, some mobile belts were strongly deformed, metamorphosed and migmatized, with ore mineralizations characterizing the late stage of the orogenic cycle (e.g. Kroner and Stern 2004; Dada 2008). The Dahomeyides belt is a 2000-km-long exposure in the southeastern part of the Tran-Saharan Belt; cutting across Nigeria, Bénin, Togo and the southeastern parts of Ghana. The belt is mainly made up of three thrust sheets (west to east; Fig. 1b): (1) the external zone composed of the deformed edge of the West African craton comprising augen

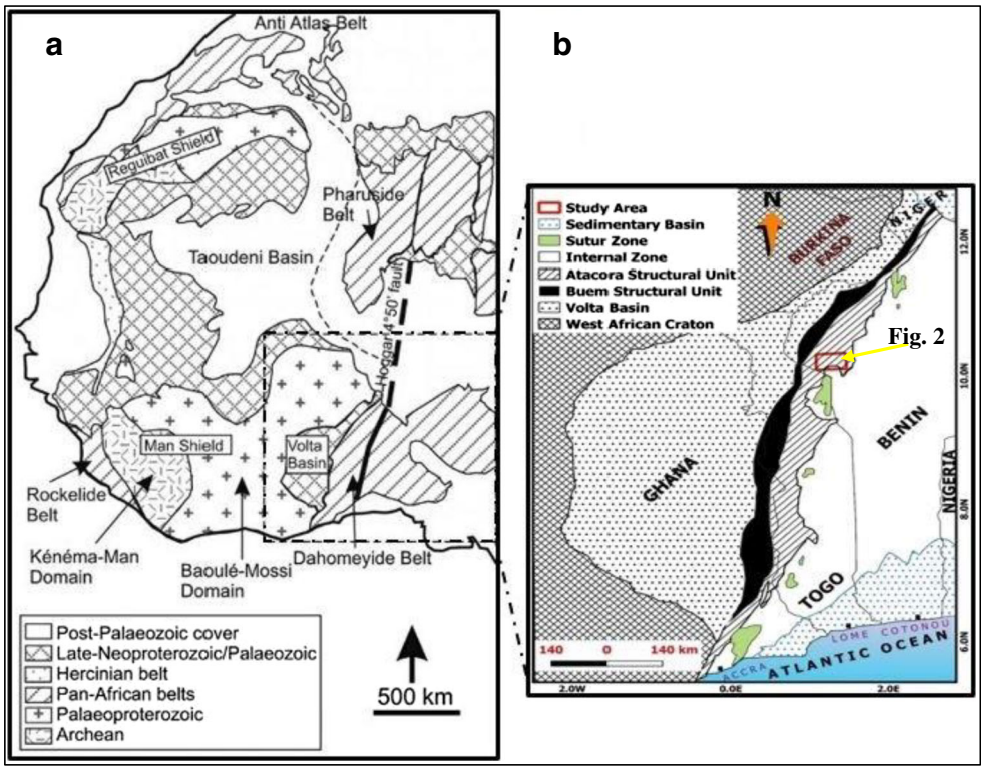

Fig. 1 **a** Map of the Pan-African belts of the West African Craton, modified after Feybesse and Milési (1994). **b** Geological map of the Dahomeyides belt showing the study area, modified after Affaton et al. (1991)

gneisses, protomylonites and granodiorites, the Buem and Atacora structural units; (2) suture zone, consisting of submeridian high-pressure and ultra-high-pressure metamorphic basic to ultrabasic rocks; and (3) internal zone (Dahomeyan structural unit) comprising migmatitic gneisses and migmatitic granite rocks. Buem structural unit comprises in part sediments of the Volta Basin, which represents the foreland of the belt. The Atacora structural unit consists of a succession of hills and ridges, from Niger River, SW of Niger Republic and extends along the northwestern Benin, Togo and Ghana border where it is called the Togo structural unit (Affaton et al. 1991; Castaing et al. 1993). The study area belongs to this Atacora structural unit and mainly consists of stacks of Neoproterozoic quartzites interbedded with schists and mica schists. These rocks display low-grade metamorphism and reflect orogenic and collisional activities during the Pan-African Orogeny. They are deformed by large tectonic structures such as crushing zones, intersection points of faults, junction points between the internal zone and the Atacora rocks. Two NE-SW to ENE-WSW trending thrust faults cross-cut the studied area (Fig. 2). A few radiometric data available on the Atacora rocks reveal only the Pan-African event, with rather diversified ages. Attoh et al. (1997) defined the limits of 579.4 ± 0.8 Ma and 608 ± 1.2 Ma on the Atacora quartzite ($^{40}Ar/^{39}Ar$ on muscovite) and proposed that the setting up of nappes corresponded to the youngest age of 575 Ma. Ganade de Araujo et al. (2016) discovered Palaeoproterozoic zircon grains in muscovite quartzite, with the youngest yielding a $^{207}Pb/^{206}Pb$ age of 1759 ± 53 Ma, while chlorite–sericite schist show Neoproterozoic ages spanning 662 to 597 Ma with a well-defined peak at ca. 649 Ma.

Sampling and analytical methods

Geological mapping of the study area (Fig. 2) and representative unweathered samples collection were carried out. Thin sections of rock samples collected were prepared at the Department of Geology, Obafemi Awolowo University, Ile-Ife, Nigeria, and were studied under the petrographic microscope at the Department of Geology, University of Ibadan, Nigeria. The structural data obtained were processed using the Geo Orient software to characterize the major trends of the host lithologies and structural deformations.

Representative samples of quartzites (n = 5) and mica schists/schist (n = 7) were selected, crushed, pulverized to below 200 mesh, packaged and sent to Bureau Veritas Commodities Ltd (ACME Laboratories), Vancouver, Canada, for geochemical analysis. 0.2 g of each sample was mixed with lithium metaborate/tetraborate and fused in a furnace at 1025 °C for their decomposition. Major elements

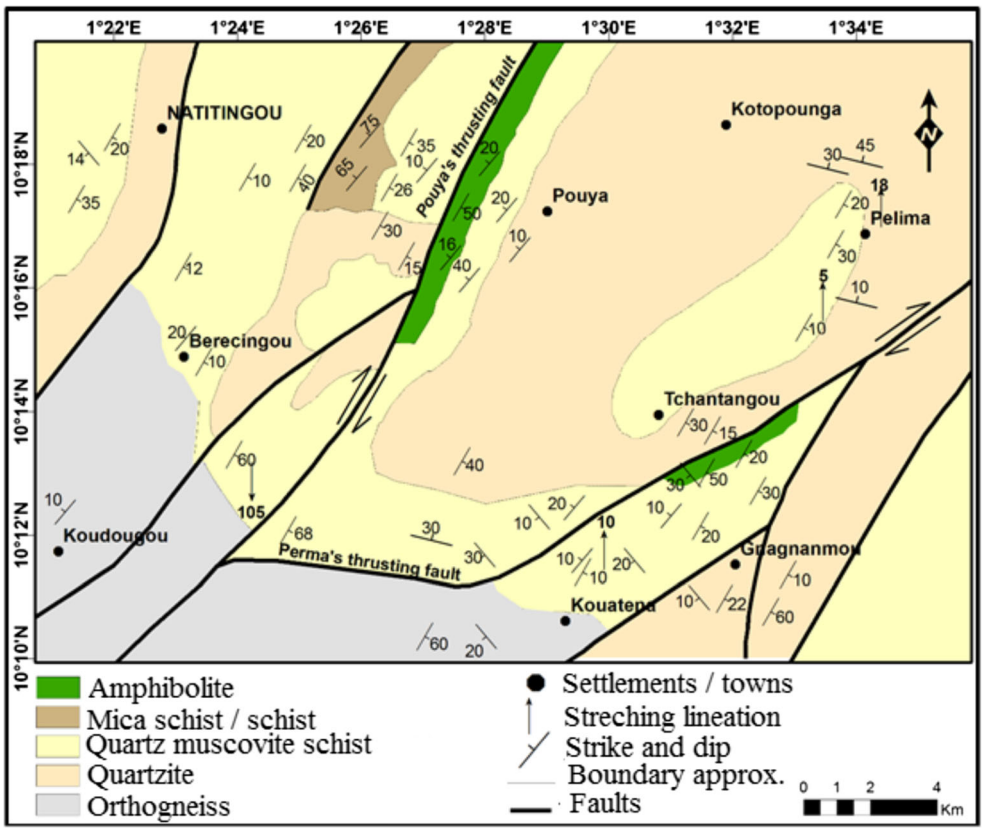

Fig. 2 Geological map of the study area

compositions of the rocks were determined by inductively-coupled plasma emission spectrophotometry (ICP-ES) with detection limits ranging between 0.002 and 0.01 percent. LOI was calculated by weight difference after ignition at 1025 °C. Trace and rare earth elements compositions were determined using inductively-coupled plasma-mass spectrometer (ICP-MS) with detection limits varying from 0.01 to 0.02 ppm for most elements and specifically 0.5 ppb for Au. The results obtained were analysed using statistical methods. During the analyses, the reference materials such as STD GS311-1, DS11, OREAS262, GS910-4, SO-19 and STD GBM309-15 were used.

Results

Field relationships and petrography

The area studied is underlined by quartzites, mica schists, amphibolites and muscovite–biotite gneiss. These lithologies outcrop at decametre to kilometre scale. Field descriptions, structural features and petrographic and geochemical analysis of the metasedimentary rocks are presented below.

Quartzite/quartz muscovite schist

Quartzite is the dominant rock type cropping within the study area, occupying about 80% of the mapped area. They occur as blocks, with dimensions ranging from 1 to > 10 m. Two types of quartzites were distinguished, namely, quartzite and quartz muscovite schist. Both types are spatially associated, with no distinguishable contact between them, suggesting they are the same rock with variation in the amount of muscovite present. These lithologies are mylonitized at the contact zones with the orthogneiss suites. In places, the quartz muscovite schist includes centimetric folded schist intercalations and concordant quartz veins in-filling the fractures within the rock. In hand-specimen, they are yellowish and pinkish (quartz muscovite schist) or brownish and greyish (quartzite) and are generally medium to coarse-grained. In thin sections, the quartz muscovite schists have grano-lepidoblastic texture with fine to medium grains that are occasionally coarse and stretched. Quartz, muscovite and opaque minerals constitute the dominant minerals in the quartz muscovite schist (Fig. 3a). The modal composition of the studied sample is in order of 82–89% quartz, 9–16% muscovite, 1% chlorite and 1–2% pyrite + magnetite .On the other hand, the quartzites are medium to coarse-grained and composed of quartz (92–95%), microcline (5–8%), plagioclase (3–5%), accessory muscovite (1–2%) and chlorite (0.7–1%) (Fig. 3b). In these quartzites, quartz occur both as recrystallized and deformed. Muscovite often appears in intergranular joints and sometimes as overgrowth of others minerals as is also chlorite. Microcline and plagioclase are dominant and form a continuous network of crystals.

Mica schist/schist

Small outcrops of the mica schist/schist are intercalated with quartzites in the shear zones. These shear zone-related mica schist occur around Pouya and mark the thrust soles of amphibolite over quartzite. They are lepidoblastic, medium to coarse-grained and light-green to light-grey. They are found at places as weathered outcrops of greyish to greyish-brown colour and occasionally contain syn-schistose quartz veinlets and exudation quartz. In thin section, the mica schist has a matrix dominated by muscovite flakes (22–46%), biotite (6–18%) and polycrystalline quartz (18–35%) aligned sub-parallel to the foliation planes (Fig. 3c). Other mineral constituents include garnet (0–10%), chlorite (2–8%), ilmenite (1–3%), plagioclase (0–4%), microcline (0–3%) and epidote (0–1%) (Fig. 3d) Biotite is dominant and chloritized, forming a continuous network in some samples. Quartz occurs as deformed grains, with muscovite inclusion. Plagioclase and microcline are sericitized with only minor relicts visible whereas garnet is very deformed in some samples. Accessory magnetite, haematite, rutile, zircon, ilmenite and epidote were also observed in thin section occurring as interstitial materials or inclusion. Epidote is probably a product introduced into the mica schist from the amphibolites around them.

Mineralized quartz veins

Mineralized quartz veins cross-cut the ASU metasedimentary rocks. The geochemical characteristics of auriferous quartz veins are not the focus in this contribution. The quartz veins are usually white, milky or smokey. They are either concordant or discordant to the main foliation in the host rocks. The concordant veins are generally mineralized and typically thinner, whereas discordant veins may be mineralized or barren. The highest Au grades are detected in concordant veins (personal communication with artisanal miners). The concordant veins, which can be > 1 m thick and > 90 m long, are mainly sub-parallel to the major faults of the area, generally filling fractures where three generations of quartz veins may be identified. The quartz veins of the first generation (type 1) and second generation (type 2), are associated with quartz muscovite schist and generally mineralized. Mineralized type 1 quartz veins are N 30°–35° E direction, boudinaged, brecciated and folded (Fig. 4b, c), whereas type 2 quartz veins are N 80°–100° E along the dextral shear zones, usually rectilinear and vertical (Fig. 4a). In thin section, the associated minerals in these quartz veins include quartz (96–98%), muscovite (0–3%), opaque minerals (haematite, magnetite; 0–1.5%) and fine-grained aggregates of pyrite in varying proportions. Generally, quartz crystals are polycrystalline

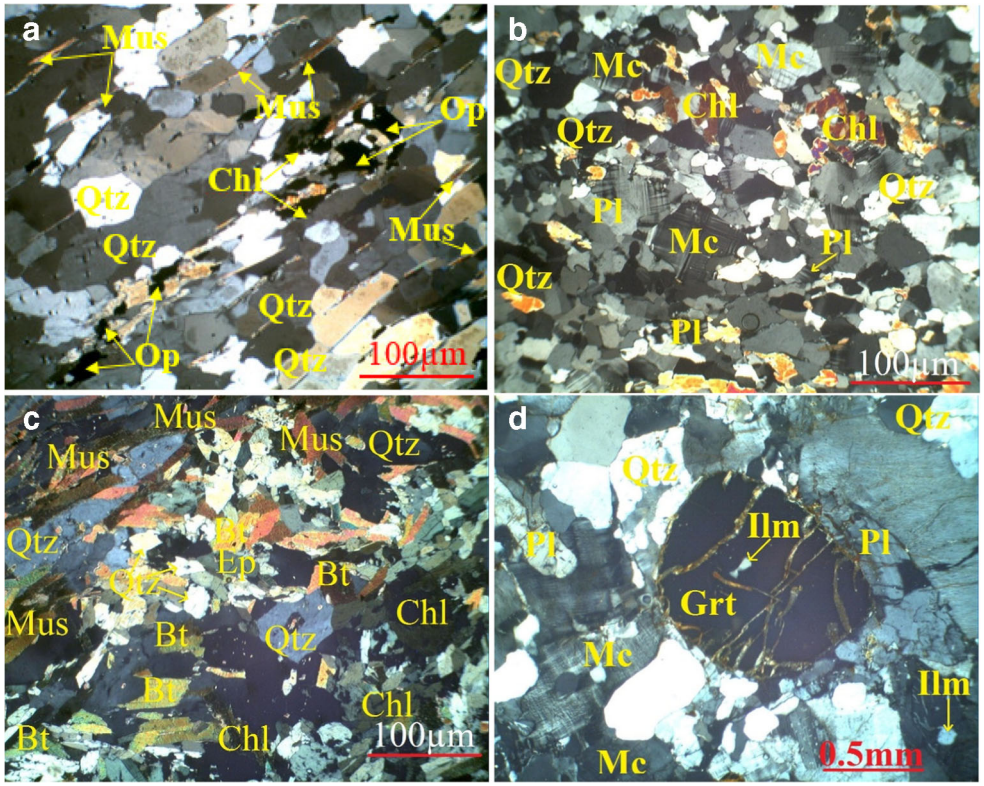

Fig. 3 Photomicrographs in transmitted light of the host lithologies showing **a** grano-lepidoblastic texture of quartz muscovite schist, **b** granoblastic texture of quartzite, **c** lepidoblastic texture of mica schist and **d** granoblastic texture of mica schist. Qtz, quartz; Mus, muscovite; Mc, microcline; Pl, plagioclase; Chl, chlorite; Bt, biotite; Grt, garnet; Ilm, ilmenite; Ep, epidote; Op, opaque minerals

with irregular grain boundaries formed due to recrystallization (Fig. 4d). Type 3 quartz veins which are barren cross-cut the type 1 and type 2 with a N 120° to N 150° W direction.

Structural features

Field mapping and systematic measurement of structural features allowed us to decipher the principal structures of the

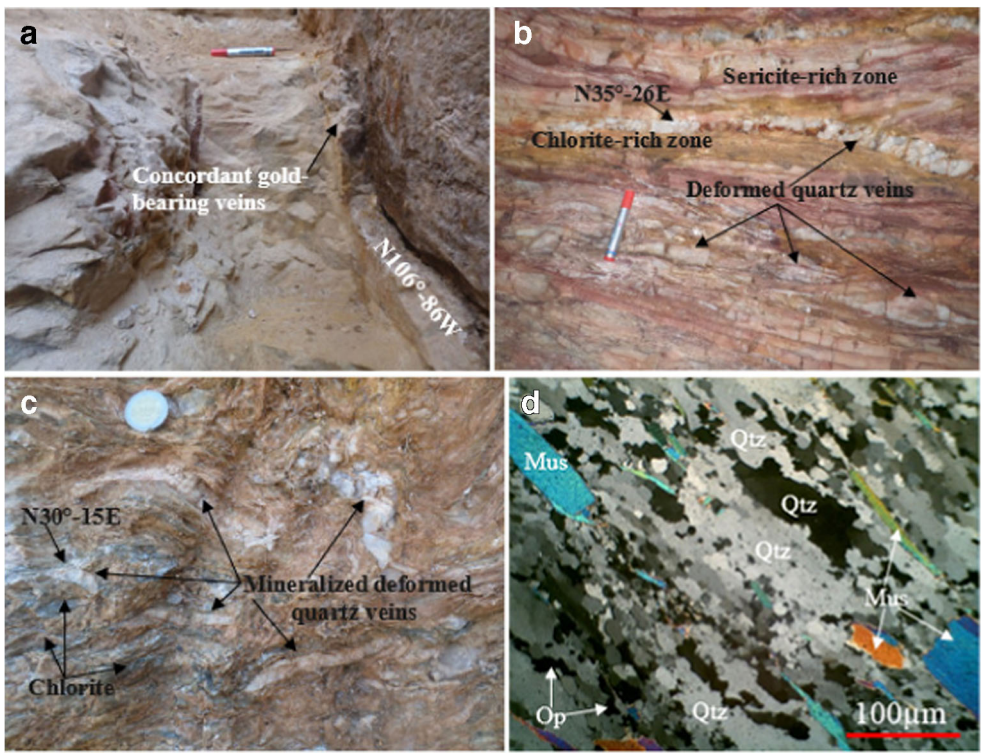

Fig. 4 **a** Field photograph showing concordant quartz veins in quartzite of the Atacora structural unit. **b**, **c** Deformed quartz lenses in quartz muscovite schist. **d** Microphotograph of gold-bearing quartz veins, crossed polarized light

study area and their relationship with gold mineralization. These characteristic structures include foliations, lineations, folds, joints, fractures and strike-slip faults.

The main structure in the field is the S_1 schistosity observed in the different lithologies. The quartz muscovite schist and mica schist have millimetric thin foliations, with an average thickness of about 4 mm (Fig. 5a). The foliations in the quartzites vary in thickness from 5 to 20 cm (Fig. 5b). The trend of foliations are NNE-SSW with low to moderate dips (5°–45°) to the east and west, with few strong dips westward (Fig. 5c). The schistosity planes bear stretching lineation, characterized by elongated minerals that plunge weakly (03°–18°) to the NE and NW (Fig. 5d). In thin section, the foliation appears as banding layers consisting of alternating light bands composed of quartz and feldspars and dark bands composed of chlorite and ferruginous materials. This alternation is often parallel to S_1 foliation and has been considered as S_0.

Two types of folds were identified in the area based on the orientation of fold axis and opening of their limbs. Centimetric to metric tight to isoclinal recumbent folds and asymmetrical to upright open folds occur in the quartzites and quartz muscovite schists. The isoclinal recumbent folds have E-W to ESE-WNW (115°–145° N) trending axial planes probably from the main NE-SW compressional stress (δ1) (Fig. 5e). Asymmetrical microfolds to upright folds have almost sub-meridian (10°–40° N) axial planar trend (Fig. 5f) with a low to medium (10°–45°) plunge. The principal compressional (δ1) stress of these folds resulted from NW-SE trend. Asymmetrical microfolds, which abundantly occur in the area, are mainly developed in the strongly deformed area where disseminated gold is being mined by small-scale artisanal workers or in abandoned trenches and excavations (Fig. 6a). These microfolds contain lenses of quartz veins of the first generation, which are mineralized and found in the

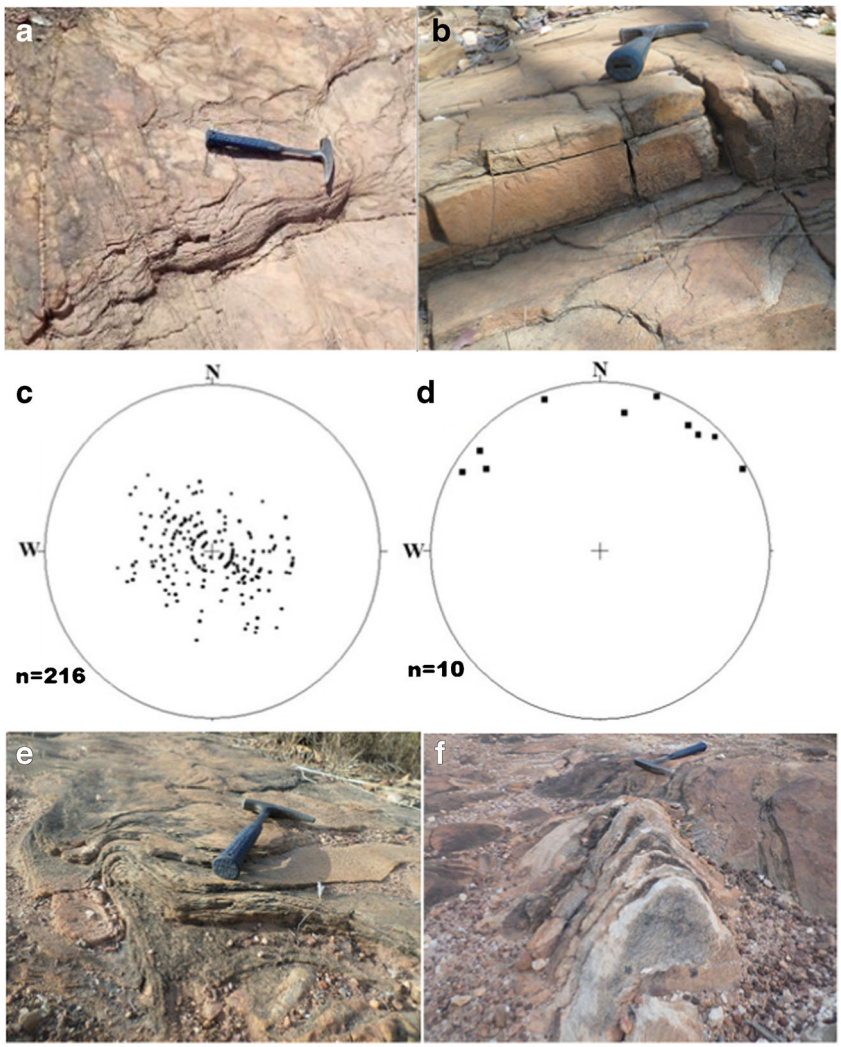

Fig. 5 **a** Field photograph showing foliated quartz muscovite schist of the ASU. **b** Field photograph foliated quartzite of the ASU. **c** Plot (full circle) of poles of foliations planes of rocks. **d** Plot of poles of L1 stretching lineation. **e** Field photograph showing F1 isoclinal fold. **f** Field photograph showing F2 asymmetric fold in the ASU metasedimentary rocks

deformed mined quartz muscovite schist rocks (Fig. 6b). Where the rocks are folded, S2 axial planar foliations are clearly observed at the microscopic scale (Fig. 6c). Around Pouya (E 001° 28′ 30″–N 10° 17′ 15″), the geometrical relationships between isoclinal recumbent folds and asymmetrical folds are remarkably visible, with the latter folds which took back the former folds in the quartz muscovite schist. Thus, the two types of folds may have resulted from two phases of folding. The first phase results in the F1 isoclinal folds with axial plane oriented in E-W to ESE-WNW while the second folding phase produced F2 asymmetric to upright open folds, displaying NE-SW trending axial planes. The F2 folds are then supposed to be younger than the F1. During the second phase of folding, the principal compressional stress (δ1) would have rotated clockwise from NE-SW to SE-NW to produce F2 asymmetric to upright folds with NE-SW trending axial planes.

Strike-slip structures are represented in the area by dextral shear planes and lenticular CS fabric. These structures are restricted to sites where mining is active and where artisanal miners worked in trenches and pits mostly in areas where the gold-bearing rocks are strongly deformed and weathered. The quartzites contain fractures healed by quartz veins which marked the C2 dextral shear, locally describing small NE-SW corridors (Fig. 6d). In the mined area, lenticular S/C fabrics resulting from NW-SE stress are also developed and defined by NE-SW direction. Gold-bearing quartz veins representing S planes in these fabrics are 45° N (Fig. 6e). In the most deformed sites, the shear plane structures occur with F2 asymmetric folds. Probably, the second folding event is contemporaneous with the major shearing episode.

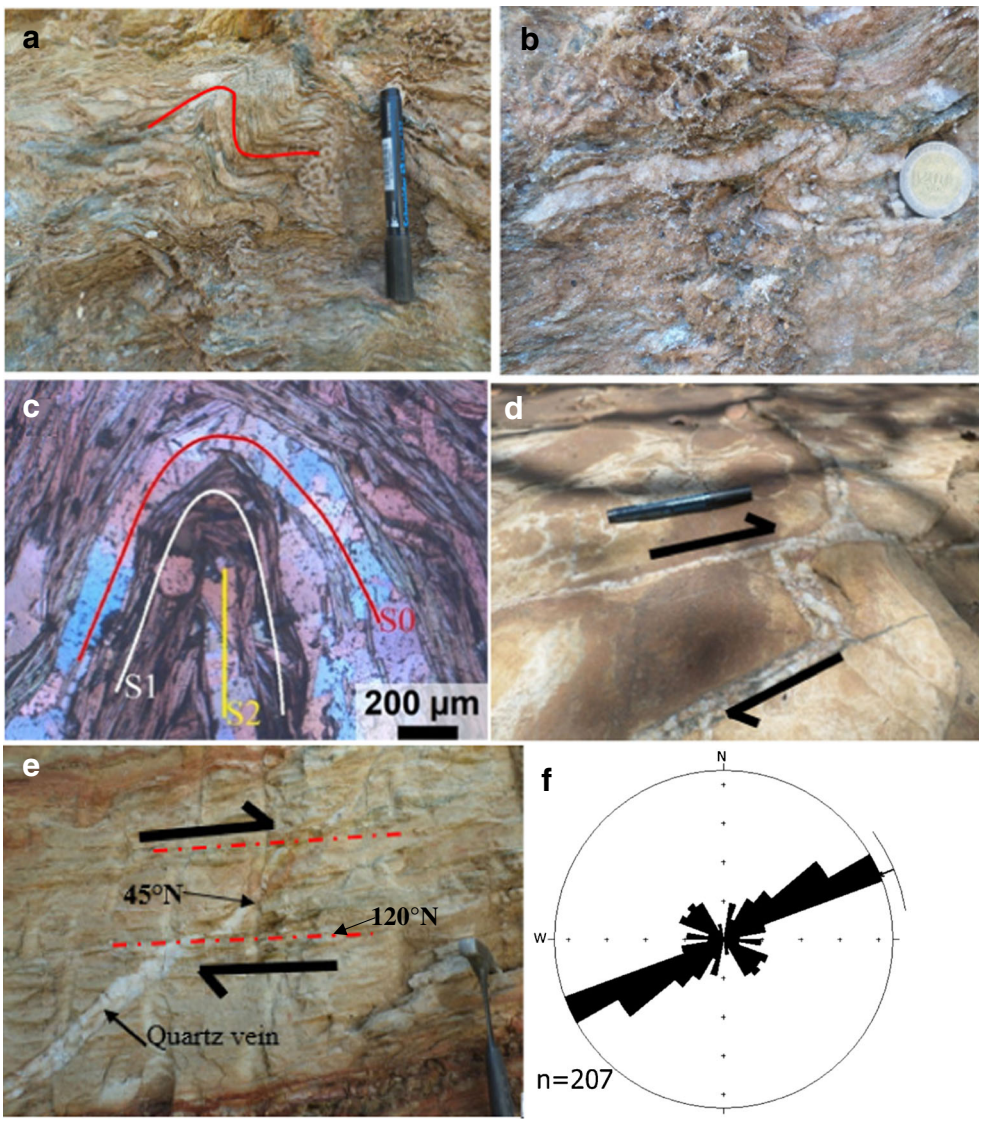

Fig. 6 **a** Field photographs and stereo plot of some structural elements in the studied rocks showing F2 fold in quartz muscovite schist and **b** F2 fold formed by quartz veinlet of S1 foliation. **c** Photomicrograph of mica schist highlighting S2 schistosity formed by the folding of S0//S1 foliation (crossed polarized light). **d** NE-SW dextral shear planes defined by different generations of quartz veins. **e** CS fabrics indicating NE-SW corridor. **f** Rose diagram of fracture planes indicating NE-SW trend

The fracture planes expressing the brittle deformation on the outcrop are metric to decametric in sizes and often healed by quartz veins. More than 207 representative fractures planes were recorded in quartzites/quartz muscovite schist and show trends in the order: NE-SW (147) > SE-NW (42) > WNW-ESE (7) > N-S (4). Thus, the major fracture trend in the study area is NE-SW trends (Fig. 6f), with northwest and southeast dips. Fault planes are mostly NE-SW and ESE-WNW and constitute the major rivers channels through the area.

Whole-rock geochemistry

Results of the major and trace element analysis of metasedimentary rocks of the ASU are presented in Table 1.

Major elements

The quartzite rock samples contain 88.27 to 94.03 wt% of SiO_2, 2.14 to 6.38 wt% of Al_2O_3, 0.07 to 0.32 wt% of TiO_2, 0.97 to 2.68 wt% of Fe_2O_3 and 0.11 to 0.16 wt% of MgO. The Na_2O and K_2O contents range from 0.12 to 0.18 wt% and 0.54 to 1.52 wt%, respectively. The CaO, P_2O_5 and MnO contents are generally less than 0.1 wt% (Table 1). The schistose rocks (mica schists/schists) are composed of SiO_2 (61.28–81.83 wt%), Al_2O_3 (8.89–17.55 wt%), Fe_2O_3 (3.31–10.5 wt%), MgO (0.18–2.55 wt%), CaO (0.01–0.88 wt%), Na_2O (0.14–0.53 wt%), K_2O (1.84–5.27 wt.%), TiO_2 (0.53–1.41 wt.%), P_2O_5 (0.02–0.23 wt%) and MnO (0.01–0.1 wt%) (Table 1). The rocks are silica-rich with an average of 90.02 wt% in quartzite (n = 5) and 72.76 wt% in schistose rocks (n = 7). Similarly, they showed appreciable TiO_2 content because of the presence of ilmenite, rutile and sphene in the rocks. The presence of iron oxide as magnetite cements gave rise to the higher Fe_2O_3 concentration in some samples. The relationships between Al_2O_3 and the other major oxides reveal a strong positive correlation of Al_2O_3 with P_2O_5, K_2O, TiO_2, Fe_2O_3 and Na_2O (Fig. 7), suggesting that the rocks are aluminous. However, increase in the amounts of K_2O with Al_2O_3 (Fig. 7) indicates that the mica, K-feldspars (microcline) and clay minerals in ASU metasedimentary rocks control the absorption of aluminium and potassium (Khanehbad et al. 2012), which could also be due to alteration.

Trace elements

The trace element content of the analysed metasedimentary rock samples from the ASU revealed that the average content of large ion lithophile elements (LILE) K, Ba, Rb, Cs and Sr are 19,744.70 ppm, 320.67 ppm, 68.17 ppm, 2.85 ppm and 41.09 ppm, respectively. In all samples, K_2O correlated positively with Ba (r = 0.90), Rb (r = 0.87), Sr (r = 0.82) and Cs (r = 0.70). This indicates that K-bearing clay minerals such as muscovite and biotite control the abundances of K, Ba, Rb and Sr in the analysed metasedimentary rocks (McLennan et al. 1993; Rollinson 1993).

However, the trace element concentrations of the studied samples are mainly below those of the Upper Continental Crust (UCC), particularly in all quartzite samples. The concentrations of Cu, Zn, Pb, Mo, Sn and Se, ranged from 2 to 33.7 ppm, 2 to 71 ppm, 0.5 to 9.2 ppm, 0.1 to 1.3 ppm, 1 to 4 ppm and 0.5 to 4.2 ppm, respectively (Table 1). These values are below the average value of the upper crust (Fig. 8a). Relatively moderate values of Ni (0.2 to 35.5), Ag (0.1–0.6), W (1–14) and As (0.5 to 11.3) ppm were recorded in the samples. Au values (average, 849.33 ppb) are notable across the samples ranging from 4.4 to 9586.8 ppb, 0.5 to 49.5 ppb and 0.5 to 464 ppb in quartzite, mica schist and schist, respectively. This distribution of gold in the studied rocks clearly indicated structural control on gold enrichment.

Rare earth elements (REE)

A summary of the REE contents in rocks of Natitingou area is presented in Table 1. The total REE and the ratio of light-REE (LREE) to heavy-REE (HREE) contents ranged from 54.67 to 501.72 ppm and 4.72 to 10.96, respectively. Enrichment in LREE, depletion in HREE and significant negative Eu anomalies (0.57–0.80) are noteworthy. When chondrite-normalized patterns of ASU rocks are compared to Post Archaean Australian Shales (PAAS) (Taylor and McLennan 1985) and UCC (Taylor and McLennan 1995), they are typically similar (Fig. 8b, c) using normalizing values from Boynton (1984). The europium anomaly parallels the depletion in Na_2O and CaO, suggesting that it developed at least partially in response to plagioclase weathering, where most of the europium is hosted. According to Taylor and McLennan (1985) and Rollinson (1993), the Eu anomaly in sedimentary rocks is usually interpreted as being inherited from igneous source rocks.

Discussion

Petrologic and geochemical characteristics

Many authors (e.g. Crook 1974; Harnois 1988) suggested that the chemical classification, provenance, tectonic settings and the extent of chemical weathering in the source area of the metasedimentary rocks can be determined using their major elements. On the Na_2O versus K_2O plot (Fig. 9a), the studied rocks plot in the quartz-rich field. As illustrated on (Fig. 9b), logarithmic plots of SiO_2/Al_2O_3 against Fe_2O_3/K_2O reveal that the quartzite can be classified as sublitharenite and subarkose, while chlorite–sericite–quartz schist and mica schist mainly have the composition of litharenite and wackes. The varied chemical composition of ASU rocks can

Table 1 Major (wt%) and trace element (ppm) composition of studied rocks in the Natitingou area

Lithology	Quartzite					Mica schist				Schists		
Sample I.D.	NT004	NT024	NT009	NT006	NT012	NT011	NT015	AD025	NT027	NT018	NT019	NT036
SiO_2	88.27	86.68	88.87	94.03	92.26	81.12	81.83	61.28	70.92	69.04	77.92	67.2
TiO_2	0.23	0.32	0.3	0.07	0.16	0.53	0.54	0.92	0.91	1.01	0.59	1.14
Al_2O_3	5.79	6.38	4.28	2.14	2.95	9.4	8.89	17.55	13.35	14.62	12.07	13.77
Fe_2O_3	1.16	1.32	2.68	0.97	1.58	4.38	4.31	6.96	7.38	7.34	3.31	10.25
Cr_2O_3	0.005	0.004	0.005	0.003	0.004	0.002	0.002	0.013	0.022	0.007	0.002	0.004
MgO	0.15	0.16	0.13	0.11	0.12	0.19	0.18	2.55	0.38	0.59	0.23	0.47
CaO	0.03	0.06	0.18	0.1	0.09	0.01	0.01	0.88	0.01	0.07	0.01	0.18
Na_2O	0.15	0.18	0.12	0.13	0.13	0.15	0.14	0.31	0.27	0.53	0.25	0.2
K_2O	1.33	1.52	0.68	0.54	0.69	1.97	1.84	5.27	4.23	3.27	3.15	4.06
P_2O_5	0.04	0.05	0.05	0.05	0.04	0.02	0.02	0.23	0.01	0.04	0.02	0.08
MnO	0.01	0.02	0.04	0.01	0.01	0.01	0.01	0.1	0.01	0.01	0.01	0.01
LOI	2.8	3.2	2.6	1.8	2	2.1	2.2	3.6	2.4	3.3	2.4	2.4
Total	99.97	99.94	99.95	99.99	99.98	99.95	99.94	99.83	99.94	99.87	99.94	99.84
Log (SiO_2/Al_2O_3)	1.18	1.13	1.32	1.64	1.50	0.94	0.96	0.54	0.73	0.67	0.81	0.69
Log (Fe_2O_3/K_2O)	− 0.06	− 0.06	0.60	0.25	0.36	0.35	0.37	0.12	0.24	0.35	0.02	0.40
CaO* + Na_2O	0.15	0.18	0.12	0.13	0.13	0.15	0.14	0.31	0.27	0.53	0.25	0.20
CIA	79.65	78.95	84.20	76.11	78.79	81.60	81.78	75.82	74.79	79.36	78.02	76.36
F1	− 8.28	− 8.27	− 7.29	− 8.52	− 8.19	− 6.42	− 6.49	− 7.89	− 6.38	− 5.19	− 7.39	− 4.83
F2	− 5.14	− 4.87	− 6.19	− 6.20	− 6.08	− 4.77	− 4.93	− 2.09	− 2.37	− 3.27	− 2.99	− 3.08
Ba	122	226	81	37	65	249	238	1104	676	200	324	526
Be	2	3	9	10	8	1	1	4	1	8	<1	4
Co	2.6	4.8	6.5	1.4	1.3	1.9	2.2	17.2	4.5	13.8	2.1	10.3
Cs	0.9	1.1	1.5	0.7	0.8	2	2.3	6.3	1.9	3.5	2.5	10.7
Hf	2.5	5.9	4.8	1.4	2	4.5	5.2	6.3	2.9	9.6	5.7	9.6
Nb	3.4	4.4	6	1.7	2.2	5.9	6.6	20.9	4.4	12.6	7.1	10.4
Rb	37	44	31	16	22	69	68	169	54	922	81	135
Sn	2	3	4	2	2	1	1	3	1	3	1	2
Sr	23	31	17	15	14	20	20	86	40	75	45	108
Th	3.5	4.9	5.4	1.6	2.3	8.3	8.7	20.3	3.8	16.3	7.1	9.4
U	0.6	1.1	1.5	0.3	0.3	1.2	1.3	2.4	0.6	2.3	1.3	2
V	15	20	20	9	9	16	18	87	81	28	29	63
W	2.3	1.8	0.8	1	1.5	3.3	3.6	3.2	2.4	6.4	13.9	1.8
Zr	105	220	180	50	68	182	194	230	108	366	223	376
Y	11.4	14.2	14.4	6.3	7.2	32	30.4	23.8	12.9	61.3	27.3	63.9
Mo	0.9	0.8	2.5	1.3	1.1	0.1	0.1	0.1	0.1	0.5	0.1	0.1
Cu	21	19	24.5	27.5	27	2	2	34	3	14	3	2.4
Pb	0.7	3	5.2	1	1	2.2	0.5	9.2	1.3	1	1.3	2
Zn	5	8	16	7	7	1	2	71	1	4	2	3
Ni	2.8	4.1	5.7	3.4	2.9	0.5	0.4	35.5	0.8	1.7	0.2	2.4
As	1.3	1.2	2.1	1.9	1.7	1.5	1.3	0.7	0.5	1.5	11.3	0.5
Sb	0.2	0.1	0.2	0.3	0.2	0.1	0.1	0.1	0.1	0.7	0.1	0.1
Au (ppb)	4.4	9587	8.8	43.2	18.9	1.1	0.5	49.4	0.5	15.3	464	0.5
K/Rb	298	289	183	278	259	236	224	259	651	296	322	249
K/Ba	90.5	55.8	69.7	121	88.1	65.7	64.1	39.6	51.9	136	80.7	64.1
Ba/Rb	3.30	5.18	2.62	2.30	2.94	3.59	3.48	6.55	12.54	2.18	3.99	3.89
Rb/Sr	1.61	1.41	1.81	1.10	1.59	3.44	3.40	1.97	1.36	1.22	1.82	1.25
La	21	21.5	19.7	12.4	11.8	27.9	29.9	39	22.3	60.8	18.3	92.5
Ce	38.5	41.2	43.7	22.1	21.1	54.6	57.5	120.6	21.3	125.4	34.9	167.4
Pr	4.99	4.86	4.56	3.06	2.76	6.43	6.77	10.44	4.98	13.75	4.3	27.59
Nd	18.2	18.2	17.8	11.8	11	25.6	26	37.2	17.6	51.3	16.2	122.2
Sm	3.07	3.25	3.23	2.2	2.03	5.47	5.57	6.63	3.64	9.46	3.18	25.4
Eu	0.69	0.72	0.59	0.42	0.48	1.42	1.42	1.31	0.91	2.29	0.76	5.56
Gd	2.44	2.83	3.06	1.67	1.85	6.22	5.97	5.51	3.29	9.73	3.71	23.08
Tb	0.36	0.44	0.44	0.23	0.27	0.97	0.97	0.81	0.49	1.66	0.7	3.16
Dy	2.06	2.54	2.72	1.32	1.45	5.97	5.49	4.98	2.82	10.38	4.6	17.16
Ho	0.42	0.53	0.52	0.27	0.29	1.2	1.14	0.99	0.5	2.27	1.01	2.9
Er	1.19	1.59	1.65	0.65	0.75	3.49	3.23	2.91	1.44	6.47	3.12	7.44
Tm	0.16	0.23	0.21	0.09	0.1	0.47	0.4	0.42	0.19	0.86	0.41	0.93
Yb	1.12	1.5	1.43	0.64	0.7	2.91	2.69	2.99	1.21	5.36	2.55	5.62
Lu	0.14	0.22	0.2	0.09	0.09	0.44	0.39	0.46	0.2	0.74	0.36	0.78
Eu/Eu*	0.77	0.73	0.67	0.67	0.76	0.74	0.75	0.66	0.80	0.73	0.68	0.70

F1 and F2 determinant factors

CIA chemical index of alteration

be related to the multiple source of the sediments and to the complexity of the stratigraphic sequence mapped. No sharp contrast between the different lithologies as evidenced by the common alternation between the schist and mica schist

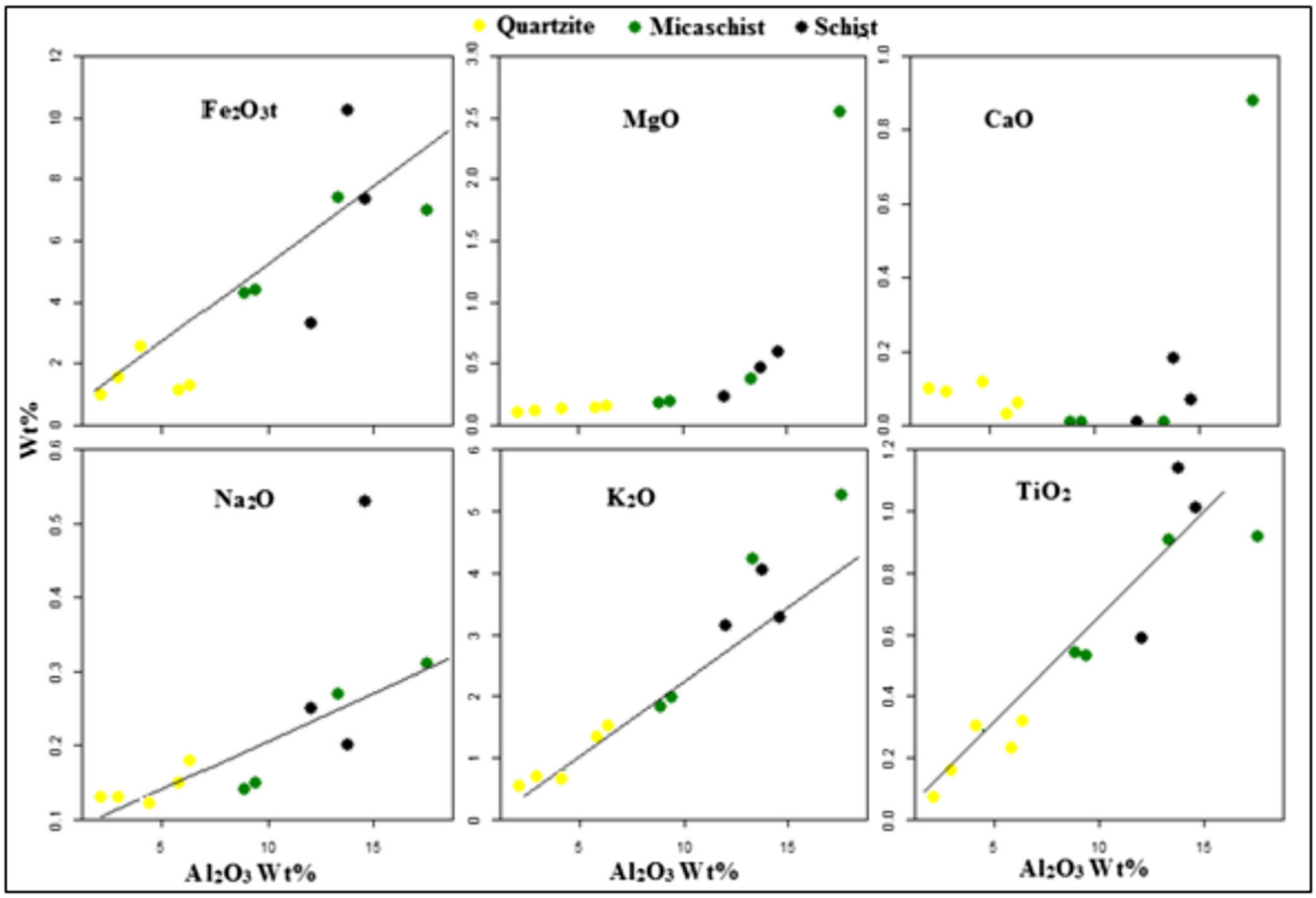

Fig. 7 Major oxides versus Al_2O_3 diagrams

outcrops intercalated within the quartzitic outcrop. By analysing the geochemical composition of sandstones and argillites from different terranes in New Zealand, Roser and Korsch (1988) proposed a series of diagrams for determining the provenance signatures of sedimentary rocks using discriminant function (DF) analysis of major element data, such as $DF_1 = A_1 \times X1 + A_2 \times X2 + A_3 \times X3 + \ldots\ldots + A_n \times Xn + C$. A, X and C represent discriminant object, coefficient and constant respectively. A are major oxides contents. X and C values are from Roser and Korsch (1988). On this discrimination function diagram, the ASU rocks plotted in the quartzose sedimentary field (Fig. 9c), indicating mature polycyclic continental sedimentary rocks. The rounded grains observed in the thin section suggested that the sediments that formed the rocks were transported to the area where they were metamorphosed. This also shows that the rocks were primarily sourced from felsic continental area, comparable to the rocks from the passive margin provenance as suggested by Anani et al. (2019).

The high quartz content of the studied rocks is probably due to the fact that the protolith was derived from felsic granitic and gneissic sources (Xu et al. 2018). This is supported by the negative Eu anomalies ranging from 0.66 to 0.80 in the studied rocks (Table 1) suggesting granitic materials as proposed by Cullers et al. (1998) and Cullers and Podkovyrov (2000). Using the approach of Rudnick (1992), the negative europium anomalies patterns on the REE diagrams (Fig. 8) support felsic source, similar to granite. Thus, it is inferred that the protoliths of these metasedimentary rocks were derived from the granitic rocks of the basement of the internal zone related to the deformed eastern margin of the West Africa Craton.

On the K_2O/Na_2O versus SiO_2 diagram proposed by Roser and Korsch (1986) to constrain tectonic setting, all the studied samples plot within the passive margin (PM) field (Fig. 9d). To determine the extent of weathering of the metasedimentary rocks, the Al_2O_3–$CaO^* + Na_2O$–K_2O (A–CN–K) plot and the chemical index of alteration (CIA) of Nesbitt and Young (1996) were used. The ASU rocks plotted in the muscovite–illite range of the A–CN–K vs CIA plot (Fig. 9e), with CIA values varying from 74.79 to 84.20% (Table 1). Values between 0 and 50% indicate fresh source areas, while values ranging from 50 to 60% and 60 to 80% indicate incipient and intermediate weathering, respectively. Values greater than or equal to 95% is equivalent to intense weathering at the source area (Nesbitt and Young 1982). CIA values obtained for the ASU rocks indicate that the source region was predominantly exposed to moderate tropical weathering (Feng et al. 2003; Ejeh et al. 2015). The values obtained are slightly

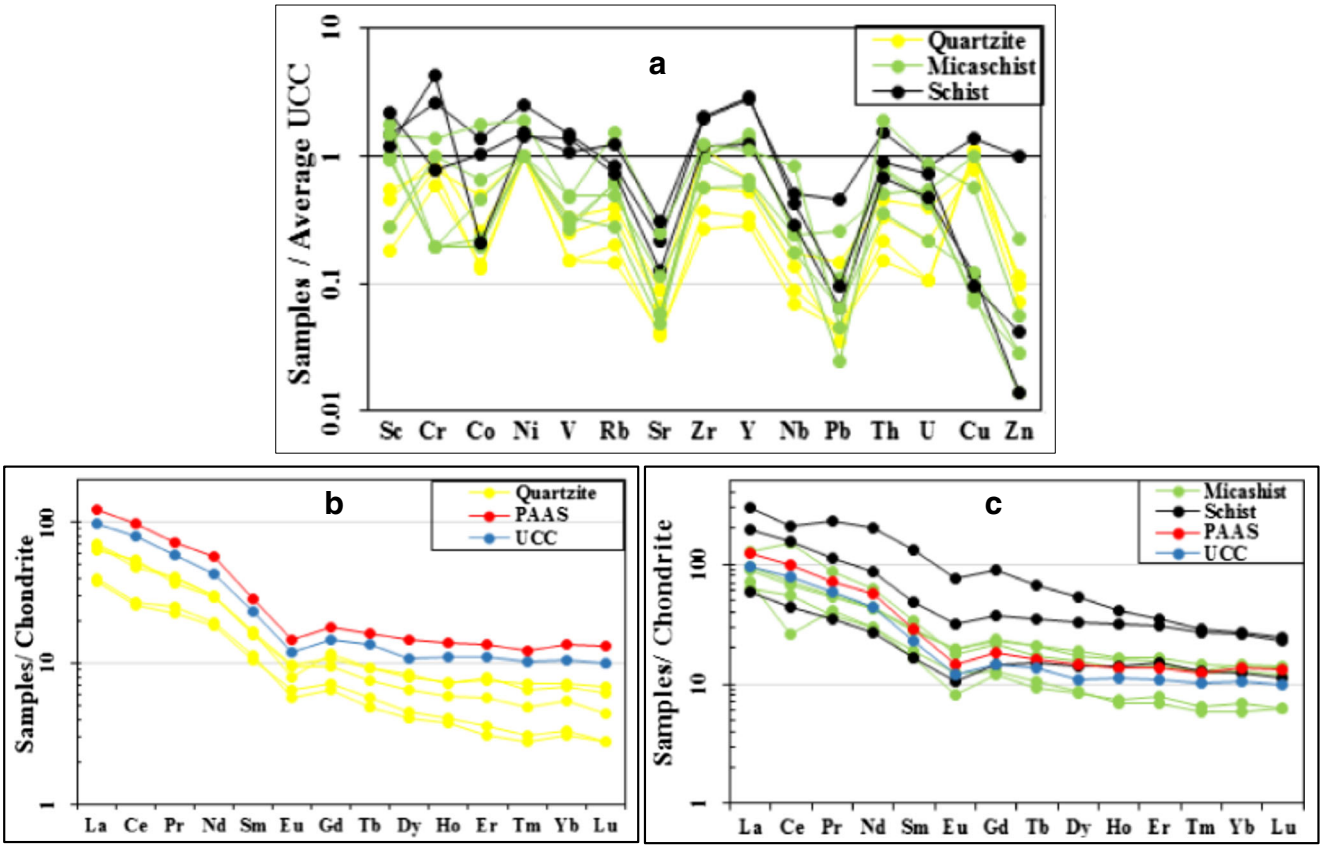

Fig. 8 Multi-elements and chondrite-normalized REE diagram for the ASU samples showing **a** multi-element diagram of studied rocks normalized against the average UCC of Taylor and McLennan (1995). **b**, **c** Chondrite-normalized REE plots for quartzite and schistose rocks, respectively, normalizing values from Boynton (1984)

higher than that of PAAS (70–75%; (Nesbitt and Young 1982; Taylor and McLennan 1985).

Mineral paragenesis and metamorphism

The mineral assemblage reported in the Natitingou area include muscovite, chlorite, biotite, microcline, epidote and garnet, which indicated greenschist facies (Turner 1981). Chlorite, muscovite and microcline often occur in all of the studied rocks. Biotite, epidote and garnet are however common to mica schist. The S1 foliation are characterized by muscovite and biotite flakes and chlorite. The chlorite is an alteration product of biotite, whereas the deformed garnet in some samples might have resulted from the reaction of chlorite + quartz. Recrystallization of quartz grains is evidenced by the subgrain rotation in quartzites, which indicated a lower temperature environment. It can be deduced that the study area has been metamorphosed to a metamorphic grade varying from lower greenschist facies characterized by the mineral assemblage of muscovite + chlorite + microcline to upper greenschist or lower amphibolite facies represented by biotite + garnet mineral assemblage (Tilley 1925; Kornprobst 1994).

Structural deformation and gold mineralization

The structural features of the rocks play an important role in the control of gold mineralization. The ASU has been interpreted as a thrust sheet resulting from the collision of the Benino-Nigerian bloc and the WAC during the Pan-African orogeny (Affaton et al. 1991). Therefore, it displayed a complex structural pattern that makes it difficult to allocate absolute chronological ages to different inventoried structures in the area. However, we attempted to determine the relative spatial relationship between these structures and mineralization. Based on the geometric aspects and superposition criteria, the structures identified in the Natitingou area are considered to have resulted from three deformational phases (D_1 to D_3), which may be related to the Pan-African orogeny. The first phase D_1 is marked by S_1 schistosity bearing L_1 lineation and folded into F_1 tight to isoclinal recumbent folds E-W to NW trending axial plane. The main compressional stress (δ1) during this folding event is probably in NE-SW. The strong folding of this S_1 corresponds to the D_2 event that is a transpressional deformation, producing initially asymmetrical to upright open F_2 folds. During this phase, the principal compressional stress (δ1) may have rotated clockwise from NE-SW to NW-SE to produce these F2 folds. The second

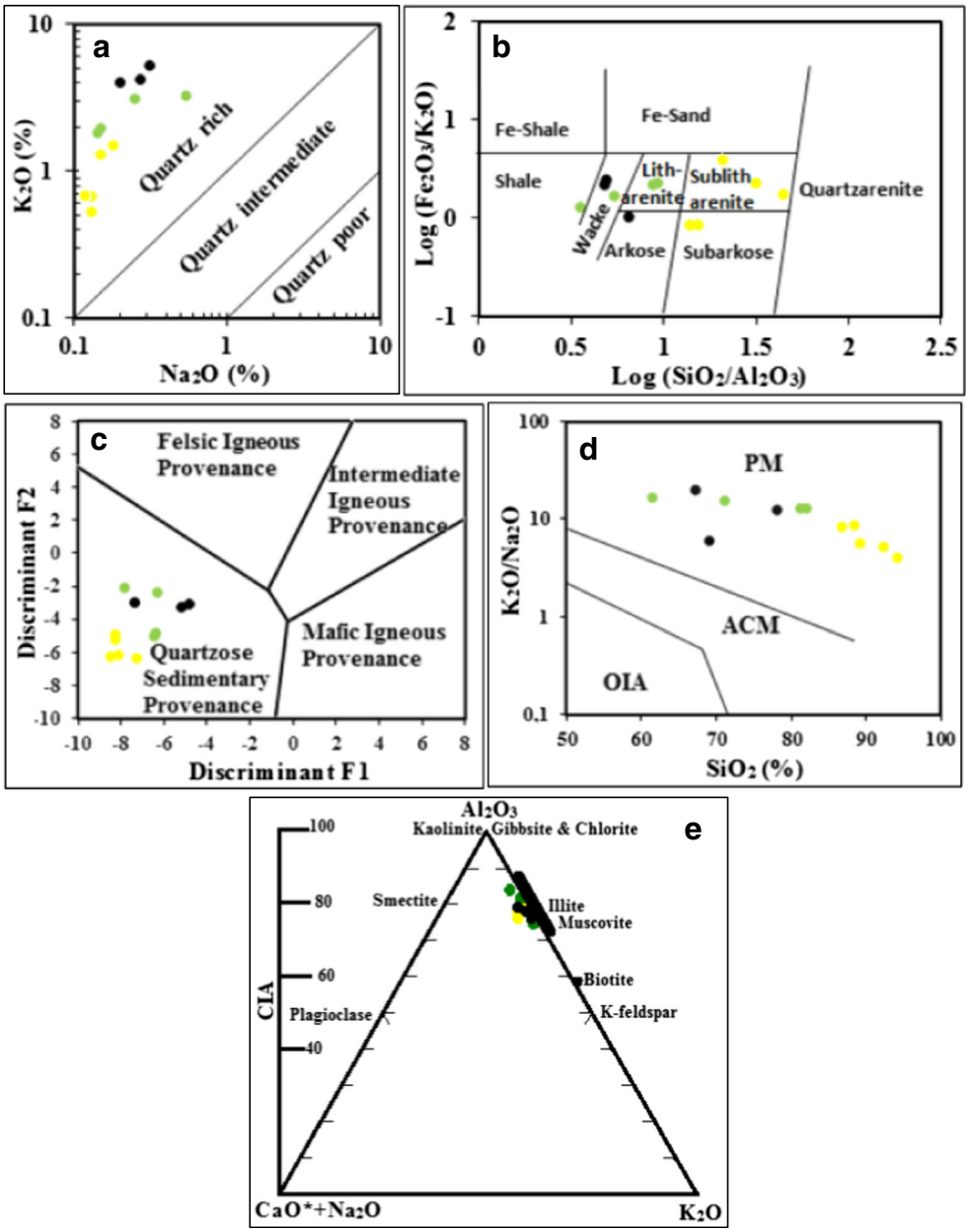

Fig. 9 Geochemical plots for the chemical classification, tectonic setting and palaeoweathering discrimination of the studied ASU rocks, showing **a** chemical classification on K_2O vs Na_2O (wt%) plot after Crook (1974), **b** chemical classification on log Fe_2O_3/K_2O against log SiO_2/Al_2O_3 plot after Harnois (1988), **c** provenance diagrams for the ASU metasediments after Roser and Korsch (1988), **d** tectonic setting on K_2O/Na_2O SiO_2 plot after Roser and Korsch (1986) and **e** weathering and CIA discrimination plot on A–CN–K plot, after Nesbitt and Young (1996) and Feng et al. (2003). (Legend: yellow, quartzite; green, mica schist; black, schist; PM, passive margin; ACM, active continental margin; OIA, oceanic island arc)

episode of D_2 produced C2 dextral NE-SW shear planes and S/C flat structures. This suggests that the two episodes of folding predated the major shearing event, which produced the NE-SW strike-slip structures. The subsequent D_3 phase notably produced NE-SW trending fractures. Zoheir et al. (2017) reported similar deformation phases in the Central Allaqi-Heiani Belt (SE Egypt), where asymmetric small scale and regional NW-SE folds are attributed to D_2 event whereas auriferous open F3 folds and NNW-SSE shear zones are related to D_3 transpressional event and NE-trending slip fault to D_4 compression and transcurrent deformation. Equally, the D_2 phase in the Natitingou area is comparable to the D_3 phase defined in Central Pharusian and Hoggar, where this D_3 phase resulted in large sub-meridian mylonitic or shear zones (Boullier 1991).

From the inventory of the different structural elements observed on the field, the mineralization in the study area is associated with characteristic structures. Gold mineralization

in the Natitingou area is chiefly disseminated within folded and sheared quartzite, mica schist and chlorite–quartz schist resulting from regional metamorphism of sediments. Where lenses of altered folded and sheared chlorite–sericite–quartz schist or mica schist occur in quartzite, gold contents was observed to increase. Gold-bearing quartz veins/veinlets hosted in these metasediments occur proximal to NE-SW strike-slip faults and NE-SW trending F_2 folds. These mineralized veins are commonly concordant to the main foliation but occasionally folded and fractured. These features suggest that gold-bearing veins were emplaced along earlier weakness zones such as shear zones, limbs and hinges of folds. Similarly, these shear zones and faults are believed to act as conduits of mineralizing fluids from the metamorphic dewatering in the amphibolite–greenschist boundary to the precipitation site of gold in the upper crust (Phillips and Powell 2010; Gaboury 2019). Therefore, NE-shear zones and faults are the primary control structures for gold deposition, whereas NE-SW-trending folds are the secondary structures favourable traps for gold deposition. According to Squire et al. (2008), the intersection between a structure and a favourable host rock can constitute geometric ore shoots. Thus, the hinge zones of asymmetric and upright folds in the Atacora metasedimentary units represents a favourable area for gold deposition. Large et al. (2011) highlighted that in orogenic gold systems, the hinge of folds may be favourable for the concentration and condensation of gold mineralization. According to Ramsay and Huber (1987) and Price and Cosgrove (1990), the hinges of folds are potential zones for gold deposition as a result of the open spaces that usually develop along fold hinges owing to geometrical advantage. Fractures are also generated during the folding phase, which are associated with compressional shear in the inner hinges, extensional shear in the outer hinges and simple shear structures along the folds limbs. It could be concluded that these brittle/ductile fractured/folded areas are potential zones for ore deposition by mineralization fluids (Groves et al. 2018). In the study area, the N-S to NE-SW compressional structures can be related to the collisional Dahomeyide orogeny, resulting from eastward subduction of WAC and westward movement of Benin Nigerian Shield. NW trending recumbent folds suggested westward movement and asymmetric to upright folds are indicative of later deformational events of the Dahomeyide orogeny. Mineralizing fluids might have migrated upwards through these compressional structures after the peak collision or after later deformation at the end of the orogeny. Thus, gold deposition appears to have taken place in the area during the late stages of the ductile, shear event of the Pan-African orogeny at ca. 600 Ma. Consequently, the shear zones may be used as a prospective guide, as it is easily recognizable in the field. This structural control characteristic identified for the gold mineralization in the ASU is identical to those highlighted by Fagbohun et al. (2020) and Araujo et al. (2002) in the Zuru Schist Belt (NW Nigeria) and the western domain of the Serido Belt (NE Brazil) respectively, where brittle–ductile structures controlled the geometry of the ore bodies.

Source of gold

Primary gold mineralization within the northern part of Benin has been linked to metamorphic and magmatic formations (Adjo et al. 2019). In this contribution, correlation, principal component and factor analyses were used to determine trace element associations with Au in the metasedimentary rocks of the Natitingou area. The correlation diagram (Table 2) of the metasedimentary rocks displayed Au–As–W–Mo association. This geochemical association is comparable to those described for orogenic gold in some other deposits (Groves et al. 2003; Goldfarb et al. 2005; Pitcairn et al. 2006b). Result of Principal Component Analysis groups gold in Factor 2 (Table 3), which is strongly associated with As–W–Cu–Mo ± Sn. This indicated a significant interaction of mineralizing fluids with the metasedimentary rock and gold precipitation in the area (Craw 2002; Groves et al. 2003; Pitcairn et al. 2006b; Dill 2010). This is supported by the REE distribution pattern of the studied samples (Fig. 8b, c), which is comparable to those of PAAS that are considered to reflect the average composition of the continental source region (Taylor and McLennan 1985). Such pattern, which was observed in the Bin Yauri phyllites and the Zuru Schist belt gold-bearing rocks in northwestern Nigeria have been interpreted to be due to extensive interaction of mineralizing fluids with metasedimentary host rocks, or that the ore fluids were possibly generated by dehydration and leaching of upper crustal rocks (Garba 1992, 2002). Additionally, gold concentrations of 43–9587 ppb in the studied rocks are higher and similar to those of other metasedimentary rocks that have abundant proportions of diagenetic primary sulphide minerals and organic matter (Pitcairn et al. 2006a; Pitcairn 2011). This suggested that the metasedimentary rocks are most probable source rocks for gold and fluids in the ASU. This view was supported by the clastic and porous nature of the studied rocks, which perhaps contained a small amount of organic matter.

A general co-enrichment and linear correlation of the large ion lithophile elements (LILE) K, Rb, Ba and Sr, coupled with inter-element ratios values such as K/Rb, K/Ba, Ba/Rb and Rb/Sr, are close to average crustal ratios of 285, 36, 7.8 and 0.12, respectively, and are characteristic features of Archean alteration domains and younger mesothermal goldfields (Kerrich and Fryer 1988; Kerrich 1989; Garba 2002). These workers used the fractionation patterns of LILE in ore deposits as tracers of the source of K and Au. K/Rb, K/Ba and Rb/Sr ratios trending towards higher values with respect to increasing concentrations of Rb and Ba, suggest mixing of the host rock and hydrothermal reservoirs of the lithophile elements (Kerrich and Fryer 1988; Kerrich 1989). In the ASU samples,

Table 2 Pearson correlation coefficient among elemental pairs

Variables	Au	Ba	Ni	Sc	Be	Co	Cs	Ga	Hf	Nb	Rb	Sn	Sr	Ta
Au	**1**													
Ba	0.0005	**1**												
Ni	− 0.1868	**0.8043**	**1**											
Sc	0.0925	**0.7037**	**0.6115**	**1**	−									
Be	− 0.3060	− 0.3817	0.0638	− 0.4219	**1**									
Co	− 0.2160	**0.6603**	**0.9336**	**0.5670**	0.1794	**1**								
Cs	− 0.0468	**0.6040**	**0.6098**	**0.7968**	− 0.1032	**0.6672**	**1**							
Ga	0.1089	**0.8316**	**0.8099**	**0.9202**	− 0.3650	**0.7684**	**0.8310**							
Hf	0.0829	0.3218	**0.5236**	**0.6820**	− 0.0700	**0.7076**	**0.7378**	**0.7309**	**1**					
Nb	− 0.0073	**0.7666**	**0.9168**	**0.5979**	− 0.0602	**0.9146**	**0.6751**	**0.8496**	**0.6727**	**1**				
Rb	0.0827	**0.8172**	**0.8211**	**0.7907**	− 0.2857	**0.7954**	**0.8510**	**0.9549**	**0.7217**	**0.9225**				
Sn	− 0.3277	− 0.0340	0.3203	− 0.2523	**0.6482**	**0.5576**	0.0736	− 0.0512	0.2760	0.3196	0.0490	**1**		
Sr	0.0300	**0.6670**	**0.7826**	**0.8440**	− 0.0698	**0.8248**	**0.9175**	**0.9121**	**0.8126**	**0.7842**	**0.8843**	0.1755	**1**	
Ta	0.0303	**0.6628**	**0.8778**	0.4920	0.0485	**0.9246**	**0.5971**	**0.7651**	**0.7040**	**0.9768**	**0.8485**	0.4625	**0.7399**	
Th	− 0.0353	**0.6456**	**0.8692**	**0.5670**	− 0.0703	**0.8736**	**0.5842**	**0.8034**	**0.7138**	**0.9664**	**0.8696**	0.2714	**0.7184**	**0.9530**
U	0.0232	**0.5244**	**0.7314**	**0.6085**	− 0.0278	**0.8654**	**0.7057**	**0.7900**	**0.8938**	**0.8987**	**0.8435**	0.3994	**0.7848**	**0.9159**
V	− 0.0506	**0.9426**	**0.7632**	**0.7869**	− 0.2937	**0.6534**	**0.6434**	**0.8200**	0.3453	**0.6584**	**0.7306**	− 0.0063	**0.7128**	**0.5566**
W	**0.9050**	0.0799	0.0401	0.2789	− 0.3518	− 0.0040	0.0300	0.3156	0.3014	0.2104	0.2617	− 0.3471	0.1878	0.2391
Zr	0.0968	0.3034	0.4959	**0.6910**	− 0.0964	**0.6811**	**0.7426**	**0.7287**	**0.9977**	**0.6500**	**0.7150**	0.2440	**0.8099**	**0.6751**
Y	0.0203	0.2045	0.4266	**0.7354**	− 0.0846	**0.5498**	**0.7441**	**0.6955**	**0.9064**	**0.5353**	**0.6547**	0.0004	**0.7638**	**0.5109**
Mo	**0.5283**	**− 0.5743**	− 0.3695	**− 0.7309**	**0.7226**	− 0.1774	− 0.4400	**− 0.6900**	− 0.3492	− 0.3889	**− 0.6185**	**0.6638**	− 0.4855	− 0.2574
Cu	− 0.3011	− 0.0138	0.2517	**− 0.5573**	**0.6589**	0.2594	− 0.2181	− 0.2949	− 0.3155	0.1367	− 0.1366	**0.6933**	− 0.1318	0.2230
Pb	− 0.1217	**0.6502**	**0.6290**	0.1082	0.0943	**0.6555**	0.3229	0.3971	0.2020	**0.7079**	**0.5460**	**0.5698**	0.3409	**0.7185**
Zn	− 0.1369	**0.6991**	**0.7460**	0.0980	0.1178	**0.6784**	0.3085	0.4320	0.1133	**0.7600**	**0.5884**	0.4610	0.3714	**0.7509**
Ni	− 0.1540	**0.7306**	**0.7691**	0.1405	0.0854	**0.6902**	0.3438	0.4673	0.1256	**0.7699**	**0.6180**	0.4289	0.4091	**0.7499**
As	**0.9832**	− 0.1375	− 0.2703	− 0.0435	− 0.1909	− 0.2837	− 0.1503	− 0.0217	0.0128	− 0.0812	− 0.0298	− 0.2838	− 0.0856	− 0.0272
Sb	− 0.1743	− 0.3361	0.2447	− 0.0468	**0.5952**	0.3284	− 0.1036	− 0.0305	0.2824	0.1190	− 0.0884	0.3737	0.1379	0.2100

Variables	Th	U	V	W	Zr	Y	Mo	Cu	Pb	Zn	Ni	As	Sb
Au													
Ba													
Ni													
Sc													
Be													
Co													
Cs													
Ga													
Hf													
Nb													
Rb													
Sn													
Sr													
Ta													
Th	**1**												
U	**0.9119**	**1**											
V	**0.5202**	0.4718	**1**										

Table 2 (continued)

W	0.2613	0.2557	0.0114	**1**												
Zr	**0.6932**	**0.8805**	0.3308	0.3137	**1**											
Y	**0.6158**	**0.7553**	0.2581	0.2882	**0.9211**	**1**										
Mo	− 0.4309	− 0.2806	− 0.4840	− 0.4273	− 0.3621	− 0.4603	**1**									
Cu	0.0539	− 0.0739	− 0.0946	− 0.4023	− 0.3512	− 0.4935	**0.5924**	**1**								
Pb	**0.5830**	**0.5493**	**0.5217**	− 0.1552	0.1701	− 0.0738	0.1122	**0.5131**	**1**							
Zn	**0.6451**	0.4844	**0.5324**	− 0.1158	0.0761	− 0.1074	− 0.0240	**0.6260**	**0.9176**	**1**						
Ni	**0.6536**	0.4838	**0.5645**	− 0.1262	0.0902	− 0.0841	− 0.0794	**0.6062**	**0.9016**	**0.9967**	**1**					
As	− 0.0917	− 0.0310	− 0.1912	**0.8832**	0.0268	− 0.0304	− 0.0973	− 0.2397	− 0.1558	− 0.1758	− 0.2033	**1**				
Sb	0.2632	0.2288	− 0.2499	0.0948	0.2740	0.3622	0.2170	0.2077	− 0.2408	− 0.1360	− 0.1455	− 0.0981	**1**			

Correlation is significant from the 0.5 level (values in bold)

these LILE elements are linearly well-correlated: K–Rb (r = 0.87), K–Ba (r = 0.90) and Ba–Rb (r = 0.81), Rb–Sr (r = 0.88) (Table 4), indicating a co-enrichment of elements contrary to those characterizing magmatic-related deposits or massive base-metal sulphide deposits of sub-marine hydrothermal source (Kerrich and Fryer 1988; Graf 1977). Moreover, the inter-element ratios obtained (Table 4) are within or close to those reported for average continental crust (Taylor and McLennan 1985), in the Canadian and the NW Nigeria gold deposits (Kerrich and Fryer 1988; Kerrich 1989; Garba 2000). The K–Rb–Ba–Sr correlation and enrichment in mineralized ASU metasedimentary rocks is controlled by the K, Rb, Ba and Sr values of the hydrothermal mineralizing fluids, apportioned in almost equitable ratios as in the source rocks (Kerrich 1989). Late-tectonic metamorphic mineralizing fluids concentrated along regional deformations are the most probable responsible factor for the remobilization of such gold mineralization through the country rocks (Kerrich and Fryer 1988; Groves et al. 2003). All these features allow us to suggest that the metasedimentary rocks are most suitable source rocks for gold and fluids in the Atacora.

As stated in the previous sections, the study area predominantly consists of thick sequences of quartzites and schistose rocks characterized by greenschist metamorphic facies. These mineralized metasedimentary rocks are clastic and relatively porous and affected by at least two deformation episodes of the late Pan-African event and thrust faults that are healed by amphibolitic rocks (Fig. 2). These structures must have offered the propitious conduits for the migration of mineralizing fluids from the metamorphic dewatering zone, in amphibolite–greenschist boundary, to the precipitation site of gold in the upper crust, while the wall-rocks provided the essential chemical elements often required for the precipitation of the gold–sulphide mineralization. In fact, during the migration of mineralizing solutions and their interaction with the wall-rocks, the dispersed gold in the sediments would be released into the solutions. Subsequently, the ore-forming materials must have migrated on an appreciable distance to form the orebodies. Clearly, shearing may have been the likely driving force for the ore forming. Therefore, it is deduced that primary gold in Atacora formations likely derived from the country rocks and remobilized by metamorphic mineralizing fluids produced during prograde metamorphism. The ores fluids migrated through the country rocks along the shear zones after the peak collision of the Pan-African Dahomeyide orogeny and subsequently channelled into depositional sites after the late deformation phase of the orogeny. In summary, the Natitingou metasedimentary rocks in the Atacora are inferred to be deposited as gold-bearing sediments, which was later remobilized after peak metamorphism of their host rocks (Groves et al. 1998; Robert et al. 2005; Groves et al. 2018) during the late Pan-African tectonic processes through metamorphic hydrothermal fluids of the upper

Table 3 Principal component analysis groups and factors

	F1	F2	F3	F4	F5	F6	F7	F8	F9	F10	F11
Au	0.0006	**0.6017**	0.2851	0.0969	0.0056	0.0082	0.0000	0.0013	0.0005	0.0000	0.0001
Ba	**0.6677**	0.0001	0.0857	0.2097	0.0002	0.0178	0.0159	0.0001	0.0027	0.0000	0.0001
Ni	**0.8393**	0.0556	0.0027	0.0002	0.0726	0.0262	0.0029	0.0001	0.0000	0.0000	0.0003
Sc	**0.5587**	0.1953	0.0873	0.0901	0.0000	0.0511	0.0131	0.0031	0.0001	0.0006	0.0007
Be	0.0162	0.3474	0.0179	**0.3766**	0.0004	0.1503	0.0335	0.0393	0.0181	0.0003	0.0000
Co	**0.8513**	0.0739	0.0094	0.0404	0.0019	0.0072	0.0131	0.0024	0.0004	0.0000	0.0000
Cs	**0.6378**	0.0239	0.0799	0.0137	0.1077	0.0417	0.0906	0.0005	0.0040	0.0002	0.0000
Ga	**0.8693**	0.0814	0.0055	0.0308	0.0011	0.0075	0.0011	0.0000	0.0033	0.0000	0.0000
Hf	**0.5591**	0.0806	0.1829	0.1077	0.0337	0.0178	0.0015	0.0073	0.0087	0.0009	0.0000
Nb	**0.9419**	0.0063	0.0155	0.0101	0.0079	0.0122	0.0006	0.0038	0.0011	0.0006	0.0000
Rb	**0.9293**	0.0277	0.0008	0.0124	0.0011	0.0025	0.0248	0.0002	0.0010	0.0002	0.0000
Sn	0.0671	**0.4478**	0.0004	0.3347	0.0860	0.0000	0.0420	0.0219	0.0000	0.0000	0.0000
Sr	**0.8007**	0.0274	0.0537	0.0011	0.0093	0.0756	0.0098	0.0209	0.0005	0.0009	0.0001
Ta	**0.8637**	0.0136	0.0194	0.0755	0.0033	0.0182	0.0009	0.0000	0.0003	0.0041	0.0010
Th	**0.8448**	0.0010	0.0000	0.0281	0.0559	0.0631	0.0001	0.0068	0.0000	0.0000	0.0001
U	**0.8037**	0.0036	0.0225	0.0928	0.0111	0.0522	0.0035	0.0090	0.0005	0.0003	0.0008
V	**0.5786**	0.0001	0.0136	0.2012	0.0033	0.1311	0.0691	0.0016	0.0000	0.0012	0.0001
W	0.0317	**0.6627**	0.1204	0.1312	0.0478	0.0016	0.0038	0.0000	0.0002	0.0001	0.0004
Zr	**0.5335**	0.1008	0.1980	0.1010	0.0368	0.0182	0.0008	0.0076	0.0033	0.0000	0.0001
Y	**0.3920**	0.1543	0.3772	0.0463	0.0001	0.0033	0.0182	0.0058	0.0010	0.0014	0.0003
Mo	0.2248	**0.3398**	0.0030	0.2500	0.1147	0.0118	0.0195	0.0178	0.0176	0.0008	0.0000
Cu	0.0001	**0.6532**	0.1618	0.0974	0.0047	0.0215	0.0234	0.0369	0.0002	0.0001	0.0008
Pb	**0.4039**	0.2303	0.2301	0.0002	0.0751	0.0197	0.0118	0.0143	0.0016	0.0129	0.0001
Zn	**0.4402**	0.2569	0.2916	0.0008	0.0003	0.0036	0.0060	0.0001	0.0000	0.0004	0.0001
Ni	**0.4701**	0.2448	0.2652	0.0055	0.0011	0.0019	0.0099	0.0008	0.0000	0.0000	0.0005
As	0.0161	**0.5199**	0.2840	0.1705	0.0027	0.0039	0.0006	0.0020	0.0000	0.0001	0.0000
Sb	0.0043	0.0246	0.1859	**0.4398**	0.3055	0.0250	0.0096	0.0000	0.0025	0.0018	0.0009

The values in bold correspond for each variable to the factor for which the cosine square is the largest

crust. The gold was precipitated as diagenetic sulphide minerals from pore water during diagenesis. Hence, these sediments constitute probable rocks source for the mineralization in the studied rocks. This geotectonic setting suggested for the Atacora gold mineralization is comparable to those of Ghana (Schmidt Mumm et al. 1997) and NE of Brazil (de Assis and Luvizotto 2018).

Consequently, the direct contribution of magmatic fluids as the source of gold mineralization in Atacora could not be substantiated in this study. This also contrasts with the view

Table 4 Correlation coefficients and summary of inter-lithophile element ratios in ASU metasedimentary rocks

Ratios	This study ASU rocks	Garba (2002) Graphitic phyllites	Kerrich (1989) Alteration domains	Taylor and McLennan (1985) Average crust
K/Rb	183–651 (295)	156–476 (204)	220–400	285
K/Ba	40–136 (77)	26–142 (49)	30–85	36
Ba/Rb	2.2–12.5 (4.4)	3–9 (4)	10	7.8
Rb/Sr	1.1–3.44 (1.8)	0.1–3 (1.6)	Erratic	0.12

Average ratios shown in parentheses

of Yessoufou et al. (2001) and El-Hadj Tidjani et al. (1997) who considered that the gold ores in the Atacora were derived from unidentified granitic pluton at depth.

Conclusions

The gold-bearing metasedimentary units at Natitingou in Atacora structural unit comprise quartzite, quartz muscovite and mica schist/schist. The various structures (foliations, lineations, folds, joints, fractures, quartz veinlets and veins, shear zones and faults) recorded in these rocks, as well as the metamorphic paragenesis that characterize them, indicated that the rocks have been subjected to ductile and brittle deformation and metamorphism during the Pan-African Orogenic event. Thin-section shows that the studied rocks are quartz-rich with moderate proportions of K-feldspar. This is also supported by geochemical analysis, which indicates that the ASU rocks are silicaclastics. They are believed to be litharenite/sublitharenite, subarkose and wackes materials, deposited in passive margin tectonic setting.

Gold mineralization is disseminated in the ductile–brittle shear and strike-slip fault zones of the metasedimentary host rocks in the Natitingou area of the Atacora structural unit. These structures could assist as a prospective guides for the search of gold in this area. It is inferred from the metals W–Cu–As–Mo ± Sn most associated with Au and large ion lithophile fractionation pattern that country rocks constitute the possible rocks source for the gold, which must have been remobilized from country rocks during the later stages of the Pan-African deformation and metamorphism and precipitated along shear conduits within the Atacora metasediments. However, future studies on fluid inclusion and stable isotope would provide more evidence on the nature and source of the mineralizing fluids.

Acknowledgements This manuscript is part of the first author's Ph.D. research at the Pan African University Life and Earth Science Institute (PAULESI), University of Ibadan, Ibadan, Nigeria. Useful comments and suggestions from the anonymous reviewers are gratefully appreciated.

Code availability Not applicable

Author contribution L.A., T.A.B., P.M.N. and F.B.A. developed the conception and design of the study. T.A.B, L.A. and P.M.N. supervised the Ph.D. thesis of F.B.A. Data were acquired in the field by F.B.A, B.A. and J.O.O., while F.A.B. wrote the manuscript. T.A.B., L.A. and P.M.N. interpreted and made the critical revision of the manuscript. All authors read and approved the final manuscript.

Funding This study was funded by the African Union Scholarship scheme, through PAULESI with matriculation number PAU-UI-0350.

Data availability Not applicable

Declarations

Competing interests The authors declare no competing interests.

References

Abdelsalam GM, Liegeois JP, Stern JR (2002) The Saharan Metacraton. J Afr Earth Sci 34:119–136

Adjo FB, Bolarinwa AT, Adissin Glodji L, Nguimatsia Dongmo FW, Olajide-Kayode JO (2019) A review of the current state of knowledge on gold mineralisation in Benin Republic, West Africa. Appl Earth Sci 128(1):2–14

Affaton P, Rahaman MA, Trompette R, Sougy J (1991) The dahomeyide orogen: tectonothermal evolution and relationships with the Volta basin. In: Dallmeyer RD, Lécorché JP (eds) The West African orogens and circum-Atlantic correlatives. Springer-Verlag, Berlin, pp 107–122

Anani CY, Bonsu S, Kwayisia D, Asiedu DK (2019) Geochemistry and provenance of Neoproterozoic metasedimentary rocks from the Togo structural unit, Southeastern Ghana. J Afr Earth Sci 153: 208–218

Araujo MNC, Alves da Silva FC, Jardim de Sa EF, Holcombe RJ (2002) Geometry and structural control of gold vein mineralizations in the Serido Belt, northeastern Brazil. J S Am Earth Sci 15:337–348

Attoh K, Dallmeyer RD, Affaton P (1997) Chronology of nappe assembly in the Pan-African Dahomeyide orogen, West Africa: evidence from 4°Ar/39Ar mineral ages. Precambrian Res 82:153–171

Black R, Latouche L, Liegeois JP, Caby R, Bertrand JM (1994) Pan-African displaced terranes in the Tuareg shield (central Sahara). Geol 22:641–644

Boullier AM (1991) The Pan-African Trans-Saharan belt in the Hoggar Shield (Algeria, Mali and Niger): a review. In: Dallmeyer RD, Lecorche JP (eds) The West African orogens and circum-Atlantic correlatives. Springer-Verlag, Berlin Heidelberg, pp 85–105

Boynton WV (1984) Cosmochemistry of the rare earth elements: meteorite studies. Henderson, P., Eds., Rare Earth Element Geochemistry. Elsev Amster, In, pp 63–114

Castaing C, Triboulet C, Feybesse JL, Chèvremont P (1993) Tectonometamorphic evolution of the Ghana, Togo and Benin in the light of the Pan-African/Brasiliano orogeny. Tectonophysics 218:323–342

Craw D (2002) Geochemistry of late metamorphic hydrothermal alteration and graphitisation of host rock, Macraes gold mine, Otago schist, New Zealand. Chem Geol 191:257–275

Crook KAW (1974) Lithogenesis and geotectonics: the significance of compositional variation in flysch arenites (graywackes). SEPM Spec Publ 19:304–310

Cullers RL, Podkovyrov VN (2000) Geochemistry of the Mesoproterozoic Lakhanda shales in southeastern Yakutia, Russia: implications for mineralogical and provenance control, and recycling. Precambrian Res 104(1-2):77–93

Dada SS (2008) Proterozoic evolution of the Nigeria–Boborema province from Pankhurst. In: Trouw RJ, Brito RAJ, Neves BB, De Wit MJ (eds) West Gondwana: Pre-Cenozoic correlations across the South Atlantic region, Geol. Soc., vol 294. Special Publications, London, pp 121–136

De Assis JAC, Luvizotto GL (2018) Gold deposits in poly-deformed metasedimentary rocks: a case study of the C1-Santaluz gold deposit, Itapicuru Greenstone Belt, Northeast of Brazil. Braz J Geol 48(4): 651–670

Dill GH (2010) The "chessboard" classification scheme of mineral deposits: mineralogy and geology from aluminum to zirconium. Earth Sci Rev 100:1–420

Ejeh OI, Akpoborie IA, Etobro AI (2015) Heavy minerals and geochemical characteristics of sandstones as indices of provenance and source area tectonics of the Ogwashi-Asaba Formation, Niger Delta Basin. Open J Geol 5(08):562–576

El-Hadj Tidjani M, Affaton P, Louis P, Lesquer P, Socohou A, Caby R (1997) Gravity characteristics of the Northern part of Dahomeyides: continental aggregation-collision orogeny and smoothing in the Pan African (600+_100 Ma). J Afr Earth Sci 17(2):203–211

Ennih N, Liégeois JP (2001) The Moroccan Anti-Atlas: the West African Craton passive margin with limited Pan-African activity. Implications for the northern limit of the craton. Precambrian Res 112:289–302

Fagbohun BJ, Omitogun AA, Bamisaiye OA, Ayoola FJ (2020) Remote detection and interpretation of structural style of the Zuru schist belt, northwest Nigeria. Geocarto Int:1–21. https://doi.org/10.1080/10106049.2020.1753822

Feng LJ, Chu XL, Zhang QR, Zhang TG (2003) CIA (chemical index of alteration) and its application in the Neoproterozoic clastic rocks. Earth Sci Front 10:539–544

Feybesse JL, Milési JP (1994) The archaean/proterozoic contact zone in West Africa: a mountain belt of décollement thrusting and folding on a continental margin related to 2.1 Ga convergence of Archaean cratons? Precambrian Res 69(1–4):199–227

Gaboury D (2019) Parameters for the formation of orogenic gold deposits. Appl Earth Sci 128:124–133. https://doi.org/10.1080/25726838.2019.1583310

Ganade de Araujo CE, Cordani UG, Agbossoumounde Y, Caby R, Basei MAS, Weinberg RF, Sato K (2016) Tightening-up NE Brazil and NW Africa connections: new U-Pb/Lu-Hf zircon data of a complete plate tectonic cycle in the Dahomey belt of the West Gondwana Orogen in Togo and Benin. Precambrian Res 276:24–42

Garba I (1992) Rare earth element study of Bin Yauri gold deposit, Nigeria. Appl Earth Sci 10:158–161

Garba I (2000) Origin of Pan-African mesothermal gold mineralisation at Bin Yauri, Nigeria. J Afr Earth Sci 31:433–449

Garba I (2002) Geochemical characteristics of the gold mineralization near Tsohon Birnin Gwari, northwestern Nigeria. Chem Erde 62:160–170

Goldfarb RJ, Groves DI (2015) Orogenic gold: common or evolving fluid and metal sources through time. Lithos 233:2–26

Goldfarb RJ, Baker T, Dubé B, Groves DI, Hart CJR, Gosselin P (2005) Distribution, character, and genesis of gold deposits in metamorphic terranes. Econ. Geol, 100th Anniversary Volume, p407–450

Graf JL (1977) REE as hydrothermal tracers during the formation of massive sulfide deposits in volcanic rocks. Econ Geol 72:527–548

Groves DI, Goldfarb RJ, Gebre-Mariam M, Robert F (1998) Orogenic gold deposits: a proposed classification in the context of their crustal distribution and relationship to other gold deposit types. Ore Geol Rev 13:7–27

Groves DI, Goldfarb RJ, Knox-Robinson CM, Ojala J, Gardoll S, Yun GY, Holyland P (2000) Late-kinematic timing of orogenic gold deposits and significance for computer-based exploration techniques with emphasis on the Yilgarn Block, Western Australia. Ore Geol Rev 17:1–38

Groves DI, Goldfarb RJ, Robert F, Hart CJR (2003) Gold deposits in metamorphic belts: overview of current understanding, outstanding problems, future research, and exploration significance. Econ Geol 98(1):1–29

Groves DI, Santosh M, Goldfarb RJ, Zhang L (2018) Structural geometry of orogenic gold deposits: implications for exploration of world-class and giant deposits. Geosci Front:1–15

Harnois L (1988) The CIW index: a new chemical index of weathering. Sediment Geol 55:319–322

Hefferan KP, Admou H, Karson JA, Saquaque A (2000) Anti-Atlas (Morocco) role in Neoproterozoic western Gondwana reconstruction. Precambrian Res 103:89–96

Kerrich R (1989) Source processes for Archean Au-Ag vein deposits: evidence from lithophile-element systematics of Hollinger-McIntyre and Buffalo Ankerite deposits, Timmins. Can J Earth Sci 26:755–781

Kerrich R, Fryer BJ (1988) Lithophile-element systematics of Archean greenstone belt Au-Ag vein deposits: implications for source processes. Can J Earth Sci 25:945–953

Khanehbad M, Moussavi-Harami R, Mahboubi A, Nadjafi M, Mahmudy Gharaie MH (2012) Geochemistry of Carboniferous sandstones (Sardar Formation), East-Central Iran: implication for provenance and tectonic setting. Acta Geol Sin 86(5):1200–1210

Kornprobst J (1994) Les roches métamorphiques et leur signification géodynamique - Précis de pétrologie, 2e édition, 228 pp

Kroner A, Stern R (2004) Pan-African orogeny. Encycl Geol 1:1–12

Large RR, Bull SW, Maslennikov VV (2011) A carbonaceous sedimentary source-rock model for carlin-type and orogenic gold deposits. Econ Geol Bull Soc Econ Geol 106(3):331–358

McLennan SM, Hemming S, McDaniel DK, Hanson GN (1993) Geochemical approaches to sedimentation, provenance, and tectonics. Processes controlling the composition of clastic sediments. In: Johnson MJ, Basu A (eds) Geological Society of America, Special Paper, vol 284, pp 21–40

Nesbitt HW, Young GM (1982) Early Proterozoic climates and plate motions inferred from major element chemistry of lutites. Nature 299:715–717

Nesbitt HW, Young GM (1996) Petrogenesis of sediments in the absence of chemical weathering: effects of abrasion and sorting on bulk composition and mineralogy. Sedimentology 43:341–358

Phillips GN, Powell R (2010) Formation of gold deposits: a metamorphic devolatilisation model. J Metamorph Geol 28:689–718

Pitcairn IK (2011) Background concentrations of gold in different rock types. Appl Earth Sci 120:1–31

Pitcairn IK, Warwick PE, Milton JA, Teagle DAH (2006a) A method for ultra-low level analysis of gold in rocks. Anal Chem 78(4):1280–1285

Pitcairn IK, Teagle DAH, Craw D, Olivo GR, Kerrich R, Brewer TS (2006b) Sources of metals in orogenic gold deposits: insights from the Otago and Alpine Schists, New Zealand. Econ Geol 101:1525–1546

Price NJ, Cosgrove JW (1990) Analysis of geological structures. Cambridge University Press, Cambridge, England

Ramsay JG, Huber MI (1987) The techniques of modern structural geology. Folds and Fractures, vol 2. Academic Press, London

Robert F, Poulson H, Cassidy KF, Hodgson CJ (2005) Gold metallogeny of the Superior and Yilgarn cratons: Economic Geology 100th Anniversary Volume. p. 1001–1034

Rollinson HR (1993) Using geochemical data: evaluation, presentation, interpretation. Longman Group, UK, pp 1–315

Roser B, Korsch R (1986) Determination of tectonic setting of sandstone-mudstone suites using content and ratio. J Geol 94(5):635–650

Roser B, Korsch R (1988) Provenance signatures of sandstone mudstone suites determined using discriminant function analysis of major-element data. Chem Geol 67(1–2):119–139

Rudnick RL (1992) Restites, Eu anomalies and the lower continental crust. Geochim Cosmochim Acta 56(3):963–970

Schmidt Mumm T, Oberthur U, Vetter U, Blenkinsop TG (1997) High CO2 content of fluid inclusions in gold mineralisations in the Ashanti Belt, Ghana: a new category of ore forming fluids? Mineral Deposita 32:107–118

Squire RJ, Robinson JA, Rawling TJ, Wilson CJL (2008) Controls on ore shoot locations and geometries at the Stawell Gold Mine, Southeastern Australia: contributions of the volcanosedimentary, alteration, and structural architecture. Econ Geol 103:1029–1041. https://doi.org/10.2113/gsecongeo.103.5.1029

Taylor SR, McLennan SM (1985) The continental crust: its composition and evolution. Blackwell Scientific Publications 312 pp

Taylor SR, McLennan SM (1995) The geochemical evolution of the continental crust. Rev Geophys 33:241–265

Tilley CE (1925) Metamorphic zones in the Southern Highlands of Scotland. Q J Geol Soc 81:100–112

Turner FJ (1981) Metamorphic petrology, 2a edn. McGraw-Hill, New York 524 p

Villenenve M, Dallmeyer RD (1987) Geodynamic evolution of the mauritanide, bassaride and rokelide origens (West Africa). Precambrian Res 37:19–28

Xu K, Ding F, Li Q, Xie X, Yang L, Li Y, Dong B (2018) Petrology and geochemistry of Upper Jurassic Weimei Formation sandstones in southern Tibet: implications for provenance and tectonic setting. Geosci J 23:1–24. https://doi.org/10.1007/s12303-018-0077-1

Yessoufou S, Trofimov NN, Yevidé H, Kaki C (2001) Genèse et conditions physico-chimiques de formations du gisement d'or de Perma dans les formations néoprotérozoique de la Chaine de l'Atacora (Bénin). Rech Scienc. Univ Lomé (Togo) 5(2):221–235

Zoheir B, Emam A, El-amawy M, Abu-alam T (2017) Auriferous shear zones in the central Allaqi-Heiani belt: orogenic gold in post- accretionary structures, SE Egypt. J Afr Earth Sci 146:118–131. https://doi.org/10.1016/j.jafrearsci.2017.10.017